Aquat Geochem
DOI 10.1007/s10498-013-9216-5

ORIGINAL PAPER

A Unified Assessment of Hydrologic and Biogeochemical Responses in Research Watersheds in Eastern Puerto Rico Using Runoff–Concentration Relations

Robert F. Stallard · Sheila F. Murphy

Received: 7 March 2013 / Accepted: 4 November 2013

Abstract An examination of the relation between runoff rate, R, and concentration, C, of twelve major constituents in four small watersheds in eastern Puerto Rico demonstrates a consistent pattern of responses. For solutes that are not substantially bioactive (alkalinity, silica, calcium, magnesium, sodium, and chloride), the log(R)–log(C) relation is almost linear and can be described as a weighted average of two sources, bedrock weathering and atmospheric deposition. The slope of the relation for each solute depends on the respective source contributions to the total river load. If a solute were strictly derived from bedrock weathering, the slope would be −0.3 to −0.4, whereas if strictly derived from atmospheric deposition, the slope would be approximately −0.1. The bioactive constituents (dissolved organic carbon, nitrate, sulfate, and potassium), which are recycled by plants and concentrated in shallow soil, demonstrate nearly flat or downward-arched log(R)–log(C) relations. The peak of the arch represents a transition from dominantly soil-matrix flow to near-surface macropore flow, and finally to overland flow. At highest observed R (80 to >90 mm/h), essentially all reactive surfaces have become wetted, and the input rate of C becomes independent of R (log(R)–log(C) slope of –1). The highest R are tenfold greater than any previous study. Slight clockwise hysteresis for many solutes in the rivers with riparian zones or substantial hyporheic flows indicates that these settings may act as mixing end-members. Particulate constituents (suspended sediment and particulate organic carbon) show slight clockwise hysteresis, indicating mobilization of stored sediment during rising stage.

Keywords Concentration-runoff relations · Watershed biogeochemistry · Tropical hydrology · Tropical biogeochemistry · Soil hydrology · Weathering processes

Electronic supplementary material The online version of this article (doi:10.1007/s10498-013-9216-5) contains supplementary material, which is available to authorized users.

R. F. Stallard (✉) · S. F. Murphy
U.S. Geological Survey, 3215 Marine St (Ste. E127), Boulder, CO 80303, USA
e-mail: stallard@usgs.gov

Published online: 06 December 2013

1 Introduction

The application of mass balance approaches in small watersheds has greatly advanced our understanding of the rates and processes that affect weathering and stream chemistry. This approach was pioneered by Owen P. Bricker III (1936–2011), who greatly influenced watershed studies at the US Geological Survey (USGS) during his 25-year tenure with the bureau. His work contributed to the founding of the USGS's Water, Energy, and Biogeochemical Budgets (WEBB) program (Baedecker and Friedman 2000), which has been evaluating the discharge of water and solutes in small watersheds at five sites across the USA, including the eastern Puerto Rico site examined here, for more than two decades. Such comparative studies of small watersheds have aided characterization of hydrologic and biogeochemical chemical processes operating at the landscape scale by controlling for geology, land cover, and climate.

Some important findings of Owen Bricker's early work included the observation that stream solute concentrations during storm events could not be explained by simple dilution and that various solutes behaved in different ways (Bricker et al. 1968; Cleaves et al. 1970). In addition, Bricker and his colleagues found that solute concentrations differed during the falling stage of a hydrograph compared to the rising stage (a phenomenon known as hysteresis). They proposed a simple weathering model whereby distinctive chemical and hydrologic responses are imparted to the stream from precipitation falling on the channel, flood plain, and upland areas. This general approach has been built upon by other researchers, and various methods have been used to attribute stream chemistry to different sources and flow paths. One such method is end-member mixing analysis (EMMA), in which the composition of the stream is assumed to result from conservative mixing of waters with distinct compositions, such as event and nonevent water (2-member mixing), or groundwater, hillslope water, and organic-horizon water (3-member mixing) (Christophersen et al. 1990; Hooper et al. 1990), or water from two contrasting land covers and a flood plain (Burns et al. 2001). EMMA has been incorporated into evaluations of the causes of hysteresis.

Hysteresis is often characterized in terms of "loops" based on the loop-like graphs of concentration (C) compared to discharge (Q) or runoff rate (R). Loops have been studied for both particulate and dissolved material. The interpretation of Q/C loops for suspended sediment is relatively straightforward: Most commonly, sediment concentrations are higher on the rising stage of the hydrograph (clockwise loop). This is because base flow has little sediment (being primarily derived from groundwater), storms lead to increased discharge and thus suspend bed sediment, and large storms convey additional sediment from bank erosion, sheetwash, gully formation, debris flows, and landslides; When the storm ends and discharge decreases, sediment drops out of the water column (Williams 1989). The lack of a loop, or a counterclockwise loop, is rarer situations; the lack of a loop is interpreted as an uninterrupted supply of sediment, whereas a counterclockwise loop is interpreted as the result of post-storm bank or slope failures or delayed inputs from upstream sources (Williams 1989).

The interpretation of Q/C loops for solutes is more complicated, presumably because a mix of subsurface and surface sources contributes solutes to streams during a storm event. Evans and Davies (1998) present a Q/C loop model for solutes based on three end-members: ground water, soil water, and event water. They use a single generic hydrograph to predict six different Q/C loops, and the rank order of the concentrations of the three end-members is uniquely related to loop type (Fig. 2 in Evans and Davies 1998). Chanat et al. (2002); however, use Monte Carlo experiments to show that even slight modifications of

this generic hydrograph result in ambiguous relations between loop type and relative end-member concentration, especially for solutes with high base flow concentrations—those of presumed bedrock origin.

Godsey et al. (2009) present observations and a model that is, in essence, a rebuttal of the reservoir-based end-member mixing approach and therefore its strict application to describing hysteresis. Godsey et al. (2009) focus on bedrock-derived chemical constituents that are not biologically active—sodium (Na^+), calcium (Ca^{2+}), magnesium (Mg^{2+}), and silica ($Si(OH)_4$)—using data from 59 small, relatively undisturbed, climatically and geochemically diverse watersheds in the USGS's Hydrologic Benchmark Network (HBN). They observe that most streams demonstrated a near-linear relation between $\log(R)$ and $\log(C)$,

$$\log(C) = a + b \cdot \log(R), \tag{1}$$

where a is a constant and b is a slope derived from the exponential coefficients for depth-dependent change of four structural and chemical soil properties. They interpret this linear relation to indicate a commonality in the physical and chemical mechanisms that mobilize and export bedrock-derived solutes from watersheds, and propose a physically based, strictly log-linear, "permeability–porosity–aperture" (PPA) model. In the PPA model, solute flux is proportional to reactive surface area such that secondary and back reactions do not control solute fluxes, and reaction rates increase at higher discharges because the wetted mineral surface area increases. Precipitation falling on the watershed is uniformly distributed, and flow through the soil is governed by Darcy's law. The model predicts that all bedrock-derived constituents should have the same slope, b. A zero slope equates to a fixed concentration and is termed a "chemostat," implying that subsoil processes increase the supply of a constituent in proportion to the volume of water passing through the soil. A slope of −1 implies a constant input rate of the constituent, independent of water throughput. A positive slope implies that increasing rainfall and runoff serve to mobilize the constituent. Many watersheds respond in a similar way, despite marked differences in geology, vegetation, and climate. For Na^+, Ca^{2+}, Mg^{2+}, and $Si(OH)_4$, b in most of the 59 rivers in the HBN is slightly negative (mostly between −0.05 and −0.15) and is statistically different from zero.

Basu et al. (2010) and Thompson et al. (2011) expand on chemostatic behavior by extending the types of constituents involved and possible mechanisms. Basu et al. (2010) argue that near-constant discharge-weighted mean annual concentrations of total nitrogen and phosphorous reflected a legacy of soil reservoirs of these constituents. Thompson et al. (2011) examine most major solutes and nutrients from nine sets of experimental watersheds encompassing 29 rivers. They use the ratio of the coefficient of variation of concentration to the coefficient of variation of discharge to characterize the degree of chemostatic response; low ratios (<0.3) indicate chemostatic behavior. Weathering derived constituents were chemostatic; nutrients were chemostatic if they demonstrated high export, indicative of a large source. Thompson et al. (2011) propose a continuously stirred linear-reaction model (CSTR), which involves a fluctuating water table and different distributions of mass storage at different soil depths to predict chemostatic behavior.

The PPA and CSTR models assume that precipitation infiltrates into and through the soil in a uniform way. However, soil is complex and can contain impermeable layers that shunt water laterally at shallow depths, or soil pipes and macropores (large-diameter connected flow paths characteristically produced by soil cracks, decayed roots, and burrows) which can provide pathways for rapid passage of storm water through soil in many

directions (Beven and Germann 1982; Jones 1990; Chappell et al. 1998; Chappell and Sherlock 2005). In addition, these models do not emphasize storms, which play a major, often dominant, role in the mobilization of river-borne materials from hillslopes and stream channels and the transport of these materials downriver (Wolman and Miller 1960). The role of storms varies with landscape and climate (Wolman and Gerson 1978) and can determine long-term average solute compositions of rivers (Stallard 1985). During storms, near-surface lateral flow through macropores and pipes and overland flow can be more important to runoff than deep soil infiltration (Elsenbeer 2001; Godsey et al. 2004).

A suitable model relating concentration to runoff rate is probably a three-stage composite model consisting of a physically based model (like the PPA model) for the deeper soil, a model that captures near-surface flow paths (modified from PPA), and a model that incorporates reservoirs that become active only at high rainfall rates (such as EMMA). The activation of the shallow flow paths during storms suggests that the examination of solute chemistry should be built around consideration of three overlapping solute sources, listed here in the order in which they become active:

1. Matrix groundwater flow, spanning from fractured bedrock to the ground surface, where the ratio of contact surface area to water volume is high, and the amount of mineral matter greatly exceeds that of organic matter (this matrix flow would be best described by the PPA model, which uses Darcy's law to describe flow through the soil).
2. The biologically active surface zone (which overlaps with the zone of matrix groundwater flow), where macropores and pipes are important. The ratio of contact surface area to water volume should be considerably less than for matrix flow, but the lateral flow distance (many meters) would be greater than that of exclusively vertical flow (less than a meter). This zone contains a mix of mineral soil, soil organic matter, and live roots and microorganisms.
3. The soil surface, where overland flow occurs during the largest storms. There are two types of overland flow: saturation overland flow, where the water table rises to the surface (typically in riparian zones and areas of flow path convergence), and infiltration-excess overland flow (surface runoff), when the rainfall rate exceeds the soil infiltration capacity. During overland flow, the ratio of contact surface area to water volume should be the least of the three solute sources. Water interacts with vegetation, litter (in varying degrees of degradation), surface roots, and microorganisms. Presumably, all reactive surfaces in and on the soil are completely wetted during the strongest overland flow.

A similar conceptualization of dual flow paths and independent soil–water reservoirs has been described by Brooks et al. (2010) for a seasonally wet temperate forest, where after the first rains of the wet season, the water transpired by plants is physically isolated from the storm water flow path. A recent study of one of the forested tropical watershed evaluated in this paper also appear to fit this model. Kurtz et al. (2011) observe a distinct hysteresis for germanium, $Si(OH)_4$, and oxygen-18 during storms in the Icacos river, and argue that rising stages are mostly mixtures of base flow and storm water, whereas water in the falling stage resembles water sampled by tension lysimeters.

To develop a comprehensive understanding of the sedimentological and biogeochemical roles of massive storm events, the solid and solute mass transport must be measured over a range of such events. However, due to logistical complexities, few studies have successfully sampled sediment and chemistry during the very large storms that occur in the tropics (Alexander et al. 1996; Goldsmith et al. 2008; Haire 1972; Hicks et al. 2000). In these studies, the highest runoff rates that were sampled and analyzed for a complete suite of

major solutes and nutrients were 9.8 mm/h in a tropical river and 12.8 mm/h in a temperate river (Stallard 2012c). Murphy and Stallard (2012a) recently published a synthesis of 15 years of data collected in four watersheds in eastern Puerto Rico encompassing a range of storm flows, including 256 samples collected at runoff rates from 10 mm/h to >90 mm/h. Chemical and sediment data at such high runoff rates are a virtually unexplored realm for biogeochemical studies of river systems. With these data, Stallard and Murphy (2012) estimate continuous rates of watershed export (load) of each constituent using the load-estimation program LOADEST (Runkel et al. 2004), average the loads for ranges of runoff in order to construct representative log(R)–log(C) relations, and show that the watersheds had considerable similarity in runoff generation and flow path structure despite differences in geology, soils, and land cover. However, the LOADEST trends are not well-suited for an in-depth examination of processes associated with solute mobilization, because the trends do not pass through the middle of the data-point cloud. In the present paper, we use log(R)–log(C) regressions to examine the presence or absence of chemostasis and to remove the overall log(R)–log(C) trend from the log(C) data to develop a test of whether rising stage log(C) is different from falling stage log(C).

In this new examination of log(R)–log(C) relations, we ask the following questions: (1) Can we refine the interpretation of log(R)–log(C) relations to clarify the processes that control constituent inputs using either PPA or EMMA types of models? (2) Are the patterns of soil hydrology and log(R)–log(C) relations consistent with a three-stage composite model, whereby successively more shallow flow paths dominate with increasing runoff rate? (3) Do patterns of hysteresis among the rivers add to our understanding of watershed dynamics gained through use of log(R)–log(C) relations?

2 Setting

Four watersheds in eastern Puerto Rico were evaluated to assess the influence of land cover, geologic, topographic, and hydrologic variability, including large storms, on a wide range of hydrologic, physical, and biogeochemical processes (Table 1, Fig. 1). Two of the watersheds are located on coarse-grained granitic rocks (Icacos and Cayaguás), and two are located on fine-grained volcanic rocks and volcaniclastic sedimentary rocks (Mameyes and Canóvanas) (Murphy et al. 2012). For each bedrock type, one watershed is covered with mature rainforest (Icacos and Mameyes); the other is undergoing reforestation after being used as agricultural land (Cayaguás and Canóvanas). The watersheds were chosen to avoid upstream tributaries with marked geologic contrasts that can complicate data interpretation. A subwatershed of the Icacos, the Guabá, was also studied to examine scaling effects. The higher-order channels in the Icacos and Cayaguás watersheds typically have thick and extensive flood plains, while channels in the Mameyes and Canóvanas watersheds have patchy flood plains, narrow riparian zones, and deep bouldery beds with a good potential for hyporheic flow. The Guabá has a bedrock channel and no riparian zone, flood plain, or bouldery beds. Shallow soils developed on both the granitic and volcaniclastic rocks, along with river-borne sediments (from which the flood plains are developed), are strongly depleted in Ca^{2+}, Na^{+}, Mg^{2+}, and potassium (K^{+}) (in order from most strongly to least) compared to the parent material (Stallard 2012b). Neither shallow soils nor bedrock contains significant chloride or sulfur. The largest storms (hurricanes and cold fronts) produce much of the annual rainfall (Murphy and Stallard 2012b) and can have profound geomorphic consequences, such as landslides, debris flows, excavation and suspension of

sediment in stream channels, and delivery of a substantial fraction of annual stream sediment load (Larsen 2012; Stallard 2012b; Stallard and Murphy 2012).

The soil structure in the study watersheds is consistent with the three-stage composite model just proposed—near-surface lateral flow is frequent, and surface runoff occurs, but is rare. The soil surface in the Luquillo forest typically has a shallow litter layer partially penetrated by fine roots. The soil immediately below has abundant fine to coarse roots and an extensive network of macropores created by roots and earthworm burrows (Larsen et al. 1999, 2012). Soil pipes are visible along cut banks and steep slopes in hillslope and alluvial soils. Field studies have found that both surface and deep soil infiltrations are faster in granitic soils than volcaniclastic soils, and the sandy, granitic soils appear to be more permeable to a greater

Table 1 Geomorphic and geographic characteristics of study watersheds

Characteristic	Canóvanas	Cayaguás	Guabá	Icacos	Mameyes
Area km^2	25.5	26.4	0.114	3.26	17.8
Minimum elevation m	70	156	633	620	83
Maximum elevation m	956	445	767	832	1,050
Mean elevation m	464	287	702	686	508
Mean hillslope of watershed	0.255	0.189	–	0.222	0.365
Mean channel slope m/m	0.151	0.12	–	0.073	0.21
Main channel length km	21.33	23.5	–	2.01	13.6
Total channel length km	34.37	49.46	–	2.91	24.02
Dominant bedrock type	Volcaniclastic	Granitic	Granitic	Granitic	Volcaniclastic
Dominant land use history	Agricultural	Agricultural	Forest	Forest	Forest

From Murphy et al. 2012; – indicates not determined

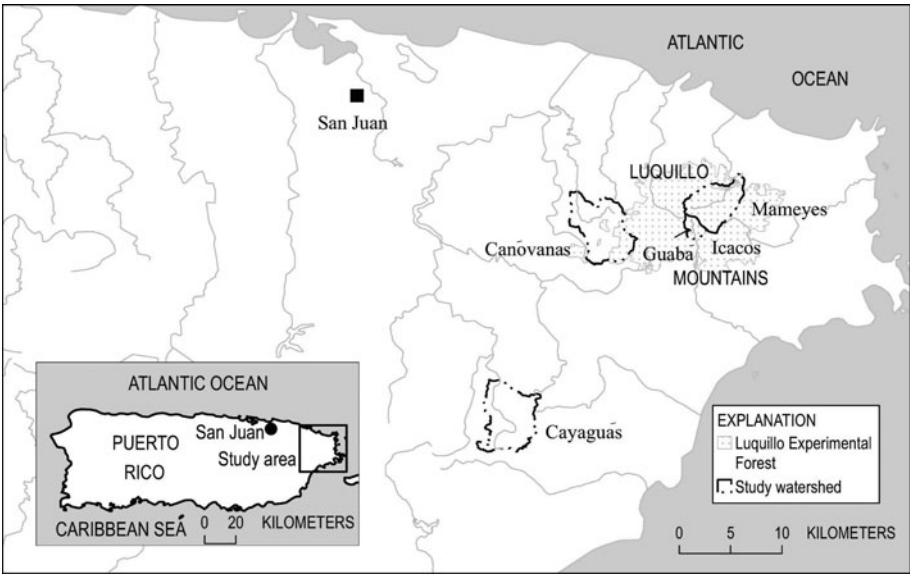

Fig. 1 Location of Puerto Rico and study watersheds

depth (Simon et al. 1990; McDowell et al. 1992; Larsen 1997). Dense clays in the volcaniclastic soils likely retard deep infiltration and cause water to follow a shallower trajectory and thus reach streams more quickly (McDowell et al. 1992). Recession models (Murphy and Stallard, 2012b) indicate that water in the deeper soil environment has about twice the contact time in the granitic watersheds than in the volcaniclastic watersheds and that groundwater storage in the soil between storms (6–100 mm) is considerably less than the amount of water delivered by large storms (>400 mm).

Both saturation overland flow and infiltration-excess overland flow (surface wash) have been observed in the Luquillo Mountains, but their relative importance has not been assessed. Saturation overland flow occurs along channels and in flow path convergence zones (Schellekens et al. 2004). On hillslopes, surface wash appears to be 1–3 % of total rainfall input and is increased by earthworm presence (Larsen et al. 1999, 2012).

Stallard and Murphy (2012) demonstrate that solute behavior in the five rivers can be classified based on their primary sources and bioactivity. Constituents that are largely bedrock-derived include Ca^{2+}, alkalinity, $Si(OH)_4$, and phosphate (PO_4^{3-}). Chloride (Cl^-) and sulfate (SO_4^{2-}) are largely of seasalt origin, although additional SO_4^{2-} comes from the weathering of sulfide minerals, and from atmospheric sulfuric acid. The cations Na^+, Mg^{2+}, and K^+ are predominantly bedrock-derived, but have substantial contributions from seasalt. Siliceous bedrock is a source of all of the bedrock-derived cations, and Na^+-bearing and Ca^{2+}-bearing bedrock-forming minerals weather the most rapidly and completely. Several constituents, such as nitrate (NO_3^-), ammonia (NH_4^+), and dissolved organic carbon (DOC), are ultimately derived from atmospheric gases (fixation) through biological, chemical, and sometimes anthropogenic mechanisms. The bioactive constituents (DOC, SO_4^{2-}, K^+, NO_3^-, NH_4^+, and PO_4^{3-}) are recycled and stored in the shallow soil environment by forest biota, and sometimes produced there as well (DOC, NO_3^-, and NH_4^+).

Despite substantial differences in land cover, annual runoff, or bedrock type, the water quality of the five rivers is not marked by extreme contrasts (Stallard and Murphy 2012). Concentrations are generally greater in the watersheds with an agricultural legacy because of less rainfall and runoff and more evapotranspiration (Table 2). These watersheds have substantially higher yields of nutrients (NO_3^-, NH_4^+, and PO_4^{3-}) and typically higher concentrations of Ca^{2+}, Na^+, Cl^-, K^+, SO_4^{2-}, NO_3^-, NH_4^+, and PO_4^{3-} at a given discharge than the forested watersheds. This suggests that additional sources, most likely human activities related to agriculture and domestic waste, contribute to this difference. In-stream biological process may cause nutrient depletion. Only the agricultural watersheds show substantial in-stream biological processes, as evidenced by carbon dioxide undersaturation and oxygen supersaturation, but this only occurs at runoff rates <0.2 mm/h when the water is clear and in-channel resident times are longer (Stallard and Murphy 2012).

3 Methods

Sampling design, analytical procedures, data quality, data processing, and the distribution of samples by time, flow regime, and type are discussed in Murphy and Stallard (2012c) and Stallard (2012c). These protocols form the basis of assessing log(R)–log(C) relations. Samples were collected both manually and with automated samplers. A preestablished discharge threshold was used to trigger automated samplers that would collect 24 samples over a 24-h period, initially at short time intervals and then expanding to several hours. This threshold had to be high enough that the automated sampler would not be triggered by

Table 2 Mean constituent concentrations and atmospheric contribution as a percentage of total bedrock and atmospheric inputs to the study watersheds, 1991–2005, ranked by atmospheric contribution

Watershed	Average annual runoff (mm/year)	Alkalinity	$Si(OH)_4$	Ca^{2+}	Mg^{2+}	Na^{+}	Cl^{-}	K^{+}	SO_4^{2-}	NO_3^{-}	NH_4^{+}	PO_4^{3-}	DOC	POC	TSS
Mean constituent concentrations (µmol/L)															
Canóvanas	970	908	366	287	198	427	332	33	45	45	3.7	0.40	321	647	435
Cayaguás	1,620	579	409	154	84	415	254	54	48	50	2.7	0.58	240	984	1,302
Guabá	3,630	165	228	51	32	192	182	16	12	11	0.8	0.05	169	629	569
Icacos	3,760	227	223	69	39	192	153	15	14	12	1.0	0.05	219	475	560
Mameyes	2,750	389	268	159	63	230	197	18	31	9	0.07	0.15	208	183	118
Atmospheric contribution (%)															
Canóvanas	970	-3	0	4	16	66	100	18	75	43/57	201	–	0/100	0/100	6/16
Cayaguás	1,620	-5	0	6	29	52	100	8	53	29/71	207	–	0/100	0/100	1/16
Guabá	3,630	-14	0	11	55	81	100	21	148	93/7	534	–	0/100	0/100	1/17
Icacos	3,760	-8	0	7	38	68	100	18	109	76/24	353	–	0/100	0/100	1/8
Mameyes	2,750	-5	0	4	30	73	100	19	65	121	582	–	0/100	0/100	1/12

Adapted from Murphy and Stallard 2012a, Table 3 and Stallard 2012b, Tables 3, 5. When two contribution values are given, the first number indicates atmospheric deposition, and the second indicates atmospheric fixation. Negative values of alkalinity indicate removal caused by acids in precipitation; values in excess of 100 % indicate that inputs exceed outputs, indicating a loss as a gas or to ecosystem accumulation

DOC indicates dissolved organic carbon, *POC* particulate organic carbon, *TSS* total suspended solids, *mm/year* millimeters per year

the hundreds of smaller storm events that occur each year (if these samples could not be retrieved before a much larger event, the larger event would be missed). As a result, samples collected during early rising stages, especially in large storms, are few in number, and late falling stages are better represented. For each sample, R and the time derivative of $\log(R)$ were estimated. If the time derivative of $\log(R)$ was positive, the sample was assigned to the rising stage, and if negative, it was assigned to the falling stage. The samples were then assigned to percentile ranges for runoff rates; each range corresponds to the fraction of total mean annual runoff that is generated by runoff rates at or below the percentile value (Stallard and Murphy 2012) (For example, the 75th percentile corresponds to the runoff rate below which 75 % of runoff in an average year is discharged). To ensure that enough samples fell into a given interval for statistical tests, a subset of the percentiles of Murphy and Stallard (2012a) are used here: 0 to <25 %, 25 to <75 %, 75 to <90 %, and 90–100 % (Table 3).

We examine a broad suite of constituents from Stallard and Murphy (2012) and Stallard (2012b), excluding PO_4^{3-} and NH_4^+ in discussions of hysteresis because the number of samples collected at intermediate runoff rates was insufficient for statistical tests. Several anomalous types of water quality samples have been identified (Stallard and Murphy 2012), and solute concentrations deemed anomalous in these samples were not included in load calculations and regressions (graphs of select constituents in the Icacos, with anomalous samples indicated, are shown in Fig. 2; for other constituents and other rivers see Online Resource 1). These included Cl^- in samples with very high Cl^- concentrations, which were associated with some hurricanes and other large storms. High Cl^- samples were also associated with elevated concentrations of other ions that are abundant in seasalt (Na^+, K^+, Mg^{2+}, Ca^{2+}, SO_4^{2-}), and often anomalously low NO_3^- concentrations. Potassium was excluded from occasional high-K^+ event samples, which were collected after Hurricane Georges (the largest storm of the study period). These samples lacked correspondingly high concentrations of Cl^- and other seasalt-related ions, and may indicate the release of K^+ from litter deposited by the storm. Finally, we excluded silica in samples with anomalously low concentrations of silica that were collected in the forested watersheds prior to Hurricane Georges, but not after; these samples may be related to an increase in shallow flow paths during some storms.

For each constituent and watershed, a first- or second-order regression between runoff and concentration was calculated:

$$\log(C') = a + b \cdot \log(R), \tag{2}$$

$$\log(C') = a + b \cdot \log(R) + c \cdot \log(R)^2, \tag{3}$$

where a, b, and c are regression constants, and C' is a predicted concentration. The second-order regression was selected in preference to the first-order using an f-test (Bevington and Robinson 2003) at a 70 % threshold (Table 4). This contrasts with the 95 % threshold used by Stallard and Murphy (2012) and was chosen because many of the relations between $\log(R)$ and $\log(C)$ have obvious curvature that is not significant at a 95 % threshold. For a few constituents, neither first-order regression nor second-order regression explained much variance; LOADEST, which accounts for temporal trends and seasonality, explains significantly more variance for these constituents. Average concentrations calculated using LOADEST (Table 3 in Stallard and Murphy 2012) were used for these constituents.

The slope (first derivative) of the $\log(R)$–$\log(C)$ relation at the 50th percentile of runoff (Table 3) for each regression is included in Table 4 for comparison among study rivers and

Table 3 Runoff rates from study watersheds at percentiles of mean annual runoff volume, 1991–2005

Watershed	Minimum runoff	Percentile of annual runoff volume				Maximum runoff
		25	50	75	90	
Runoff rate (mm/h)						
Canóvanas	0.0093	0.083	0.25	1.4	8.1	66
Cayaguás	0.020	0.11	0.27	1.8	7.8	54
Guabá	0.036	0.29	0.48	1.8	11	98
Icacos	0.059	0.29	0.57	2.1	7.5	85
Mameyes	0.024	0.22	0.46	1.5	4.9	86
Time spent below given runoff rate (%)						
Canóvanas	0	72	93	93.3	99.94	100
Cayaguás	0	63	91	99.0	99.89	100
Guabá	0	55	84	98	99.82	100
Icacos	0	57	86	98	99.67	100
Mameyes	0	59	86	98	99.68	100

Adapted from Murphy and Stallard (2012b)

with Godsey et al. (2009). The 50th percentile (runoff rates 0.25–0.57 mm/h depending on the river) was chosen because some of the log(R)–log(C) relations have slight curvature, and to be rigorously compared to the PPA model, water should be moving through deeper soil as matrix flow but not substantially through shallow-soil or overland flow paths. Assuming that water at runoff rates greater than the peak in the log(R)–log(DOC) relation (2.6–7.6 mm/h, depending on the river) represents substantial shallow-soil or overland flow, the 50th percentile, being less than the peak, is appropriate for comparison. Moreover, the rivers flow at runoff rates below the 50th percentile runoff rate 84–93 % of the time, depending on the river (Table 3). This runoff rate would therefore represent waters that are typically sampled as periodic time series, such as the HBN dataset (Murdoch et al. 2005).

To assess hysteresis, the value of log(C') estimated for each sample by the selected regression (Table 4, Fig. 2, Online Resource 1) was subtracted from the observed log(C) to obtain a normalized value, log(C/C'), which in essence removes the effect of the response of log(C) to changing runoff rates across each percentile range. For each percentile range, the normalized values of rising stage samples, subscript $_R$, log($C_R/C_R{}'$) and those of falling stage, subscript $_F$, log($C_F/C_F{}'$) were averaged separately to determine rising stage and falling stage normalized averages, C_R and C_F. The significance of the difference between these averages was evaluated with a T test (Bevington and Robinson 2003) and ranked as nominally significant (>50 %), significant (≥90 %), and highly significant (≥99 %). For those samples with a level of significance of 50 % or greater, the percentage difference between C_R and C_F was calculated as a percentage of C_R ($100{\cdot}(C_R{-}C_F)/C_R$)) (Table 5).

4 Discussion

By distinguishing among sources—bedrock weathering, atmospheric deposition, and biological fixation from the gas phase—along with estimating a level of bioactivity, a suite

of mechanisms controlling log(R)–log(C) relations can be postulated. The discussion is divided into three parts. First, the non-bioactive solutes are examined, focusing on how these relations compare to the predictions of the Godsey et al. (2009) PPA model, and hysteresis is discussed. Next, bioactive solutes are examined, using DOC as a model solute. Finally, we evaluate the particulate constituents, suspended solids, and POC, which demonstrate different responses than the solutes. Space limitations prevent graphical presentation of the regressions other than those in Fig. 2; graphs of primary data and regressions for all rivers are presented in Online Resource 1.

4.1 Relations Between log(R) and log(C) for Non-bioactive Constituents

The watersheds demonstrate similar trends in log(R)–log(C) regressions of most non-bioactive constituents (Table 4, Online Resource 1), suggesting considerable similarity in runoff generation and flow path structure despite differences in geology, soils, and land cover. The trends of the primary data are near-linear and negative (when low-Si and high-Cl samples are excluded), with slight curvature (coefficient c) in some cases. No trends are sigmoidal (Stallard and Murphy 2012). These observations are consistent with the PPA of Godsey et al. (2009).

The log(R)–log(C) relations of all non-bioactive constituents demonstrate negative slopes at the 50th percentile runoff rate (Table 4). As previously noted by Stallard and Murphy (2012), the slopes of the log(R)–log(C) relation at low runoff rates typically increase in the order alkalinity $<Si(OH)_4 <Ca^{2+} <Mg^{2+} <Na^{+} <Cl^{-}$ (with slight variations in order for different rivers) (Table 4). This order matches the atmospherically derived fraction of the total constituent load (Table 2). In fact, the relation between the log(R)–log(C) slope at the 50th percentile runoff rate (Table 4) and the atmospheric proportion of the total load (Table 2) is essentially linear (Fig. 3), with an overall regression having a slope of 0.26, an intercept of −0.38, and a Pearson correlation, r, of 0.84. The regressions for all individual rivers, except the Canóvanas, are quite similar, and all have an r greater than 0.75. The Icacos, Mameyes, and Guabá rivers, which drain watersheds with mature forest cover and intact soil profiles, have an r greater than 0.95. The most reasonable interpretation is that the water moving through the soil profile contains a mix of solutes derived from bedrock weathering (almost 100 % for alkalinity, $Si(OH)_4$, and Ca^{2+}) and solutes derived from atmospheric deposition but further concentrated by evapotranspiration (100 % for Cl^{-}). Accordingly, the log(R)–log(C) relation for any of these constituents would be a proportionately weighted mixture of a bedrock trend having a slope of about −0.40 and an evapotranspired water trend having a slope of about −0.10 (the average for Cl^{-} for all sites), with some trend variation among sites. This near constancy of slope, b, in a given watershed for the bedrock-derived component, is essentially a validation of the Godsey et al. (2009) PPM model for this landscape.

Because the atmospheric component is not derived from weathering reactions, it does not represent material released from reactive surfaces. Accordingly, the log(R)–log(Cl^{-}) trend presumably reflects the mixing of older evaporated water in the soil with storm water inputs, perhaps moving through rapid flow paths. This is analogous to soil–water processing described by Brooks et al. (2010). Accordingly, a storm may displace some of the water enriched in Cl^{-} by evapotranspiration, but it does not flush the bulk of this water out of the soil profile. This is best illustrated by examining Cl^{-} during hurricanes. During Hurricane Hortense (September 1996), Cl^{-} concentrations in the Mameyes river dropped from base flow concentrations of about 250 micromoles per liter (μmol/L) to about 80 μmol/L and then returned to base flow concentrations (Fig. 4 in Stallard 2012a); such a drop, followed

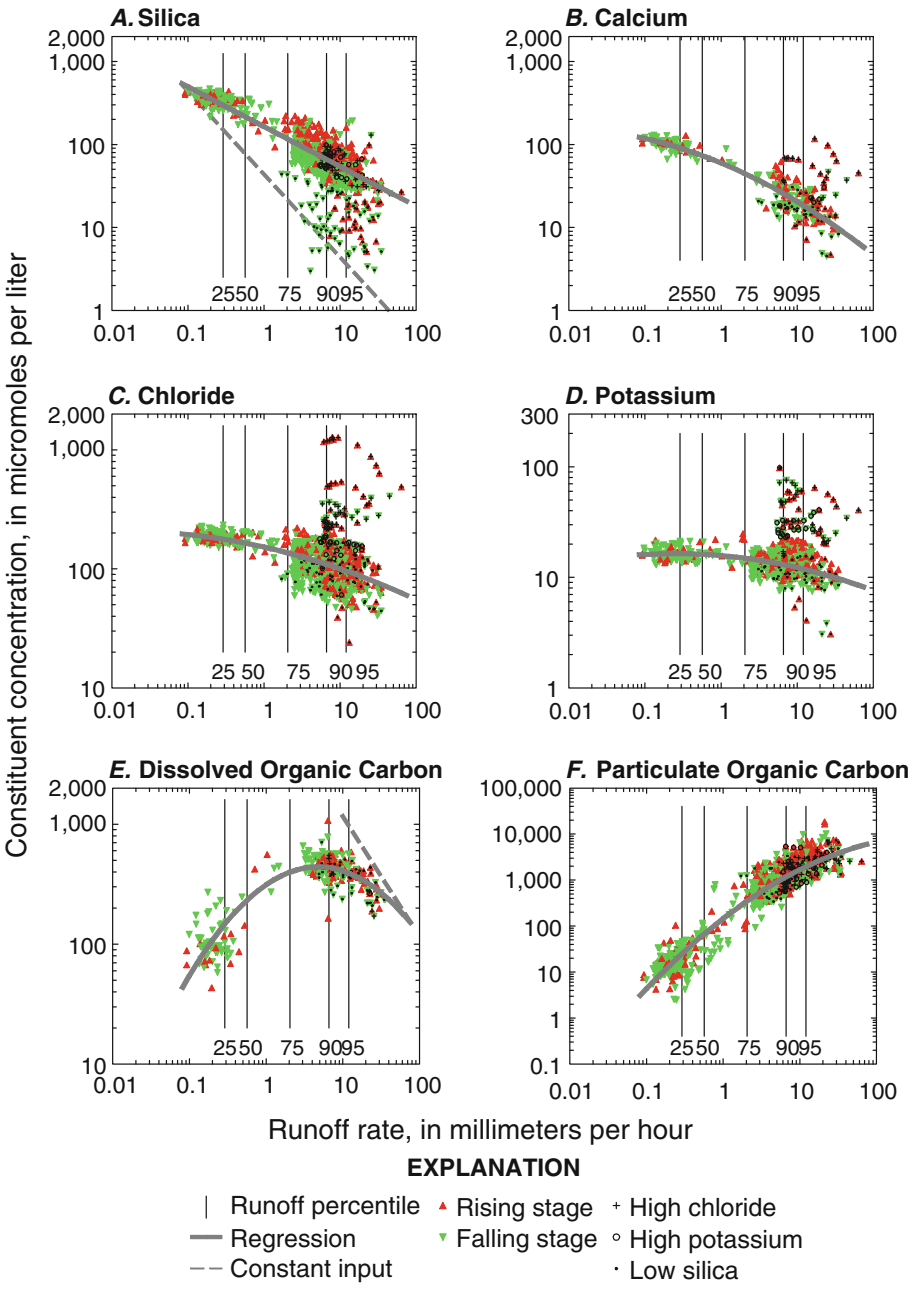

by a rise, is typical of most storms. In contrast, Hurricane Georges (September 1998) carried enough seasalt inland to raise Cl^- concentrations in the Mameyes river from base flow concentrations to more than 1,600 µmol/L after 2 h into the storm and the first 10 mm of runoff (Fig. 4 in Stallard 2012a). As the storm progressed, seasalt inputs decreased, but rain and high runoff continued; Cl^- concentrations returned to base flow concentrations after

◀**Fig. 2** Runoff rate–concentration graphs for selected constituents in the Icacos river. The lines or curves through the data are the regressions reported in this paper. Up-pointing *red triangles* indicate collection during rising stage, and down-pointing *green triangles* indicate collection during falling stage. In all panels, the high chloride symbol indicates samples with exceptionally high chloride concentrations collected during huge storms; high potassium indicates samples with high potassium but not high chloride; and low silica indicates samples with unusually low silica concentrations for the runoff rate (anomalous constituents in these three groups of samples are not included in regression models). In all panels, the vertical black lines correspond to the runoff rate below which the indicated percent of the mean annual runoff leaves the watershed. The constant input line on the silica graph (*panel* A) refers to a constant base flow supply of silica with no other sources. The constant input line on the dissolved organic carbon graph (*panel* E) refers to constant supply of dissolved organic carbon by degradation of organic matter at highest runoff rates

another 6 h and 200 mm of runoff. Whether storms have low or high Cl^- concentrations in runoff, there seems to be little net retention of a storm water Cl^- signal, and the log(*R*)–log(Cl^-) relation reflects repeated mixing of storm water with a soil–water Cl^- reservoir. Other non-bioactive constituents derived from atmospheric deposition should act similarly.

For all rivers except the Guabá, the non-bioactive constituents show generally higher concentrations during the rising stage than during the falling stage across a broad range of runoff rates (Table 5). The sampling design used in the present study, based on a stage threshold to trigger sampling, misses the rising stages of the big storms. For reference, Kurtz et al. (2011) present excellent graphs of silica hysteresis in two storms in the Icacos watershed. We were able to sample rising and falling stages of several smaller storms, and single-storm behavior matched the assessment made from grouped data. In no case do we see open, hysteresis loops typical of what is seen with sediments (Figs. 3, 4 in Williams 1989); instead, hysteresis, when manifested, involves somewhat greater or lesser concentrations on rising compared to falling stages. The largest and most statistically significant differences are observed when runoff is greater than the 25th percentile, for which alkalinity, $Si(OH)_4$, Ca^{2+}, and Mg^{2+} during the falling stage are 7–60 % less than during the rising stage. The difference is less (4–40 %) for Na^+ and Cl^-.

Because both atmospherically derived and bedrock-derived constituents are elevated on the rising stage, the source of this water is likely to be a component that has been subject to more evapotranspiration and weathering than falling stage water. One possibility is the rising stage is influenced by water derived from a flood plain or riparian zone that is displaced by storm water. Alternatively, falling stage water may be enriched in riparian outflow late in a storm. This is essentially an EMMA-type end-member following Burns et al. (2001). Riparian zones, because they store water and respond differently to rainfall inputs and rises in river stage than do hillslopes, have the potential to act as a third solute end-member (Burns et al. 2001); the lack of a riparian zone should eliminate this end-member. The Guabá watershed is the smallest watershed, only 0.114 km^2 within the 3.26 km^2 Icacos watershed (Murphy and Stallard 2012b), has the same geology, rainfall regime, and vegetation as the Icacos, but lacks a significant riparian zone or deep bouldery bed. The Guabá also has lower base flow runoff rates and higher peak runoff rates than the Icacos (into which it flows) (Table 3), consistent with the lack of a riparian contribution to runoff. The lack of a riparian zone in the Guabá watershed also suggests that the general absence of hysteresis for most solutes at all but the greatest runoff rates (Table 5) is associated with a hydrograph response that is entirely based on hillslope water storage and flow paths (an ideal PPA model river). Moreover, the lack of hysteresis at intermediate flow rates in the Guabá, in contrast to the other rivers, makes it difficult to invoke source depletion in the various hillslope flow paths that become active during a storm (Shanley et al. 2011), or multiple differentially active hillslope flow paths as proposed by Kurtz et al. (2011).

Table 4 Results of regressions for log(concentration) to log(runoff rate), with the slopes of that regression at the 50th percentile of runoff rate, and the runoff at the peak of concave-down regressions

Constituent	Regression on all measurements			Regression slope at 50th percentile runoff rate	Runoff rate at peak of arch (mm/h)	Data count	Regression percent variance explained	Best LOADEST model	LOADEST percent variance explained
	a	b	c						
Canóvanas									
Alkalinity	2.6975	−0.2996	0.0302	−0.33	–	153	76	2	76
$Si(OH)_4$	2.4171	−0.1947	–	−0.19	–	767	61	9	62
Ca^{2+}	2.2536	−0.2898	–	−0.29	–	140	82	1	82
Mg^{2+}	2.1276	−0.2575	–	−0.26	–	140	82	2	82
Na^{+}	2.5309	−0.1785	–	−0.18	–	140	80	4	81
Cl^{-}	2.4622	−0.1710	−0.0249	−0.14	–	739	52	9	54
SO_4^{2-}	1.6378	−0.0998	−0.0217	−0.07	–	145	63	9	69
K^{+}	1.5655	0.0843	−0.0551	0.15	5.8	451	45	9	49
NO_3^{-}	1.7340	0.0525	−0.2700	0.36	1.3	145	67	9	75
NH_4^{+}	(−0.5174)	(0.2747)	(0.1139)	0.10	–	85	28	6	42
PO_4^{3-}	[−0.2362]	[−0.1453]	[−0.2360]	0.00	–	133	24	8	44
DOC	2.6746	0.1002	−0.1206	0.24	2.6	315	56	8	59
POC	2.7312	0.7133	−0.1997	0.94	–	1,337	72	9	79
TSS	2.5684	0.7386	−0.2368	1.01	–	1,337	73	9	80
Cayaguás									
Alkalinity	2.3619	−0.5959	−0.0476	−0.55	–	122	87	4	88
$Si(OH)_4$	2.4904	−0.3176	−0.0333	−0.28	–	759	87	9	88
Ca^{2+}	1.9612	−0.4137	−0.0465	−0.37	–	104	88	4	89
Mg^{2+}	1.6707	−0.4042	–	−0.40	–	104	88	4	89
Na^{+}	2.4793	−0.3063	–	−0.31	–	104	93	9	94
Cl^{-}	2.3805	−0.2128	−0.0537	−0.16	–	770	80	9	85
SO_4^{2-}	1.6937	−0.0678	−0.0568	−0.01	–	108	56	2	56

Table 4 continued

Constituent	Regression on all measurements			Regression slope at 50th percentile runoff rate	Runoff rate at peak of arch (mm/h)	Data count	Regression percent variance explained	Best LOADEST model	LOADEST percent variance explained
	a	b	c						
K^+	1.8072	0.0449	−0.1017	0.15	1.7	394	42	8	44
NO_3^-	[1.6458]	[0.0027]	[−0.1792]	0.00	1.0	104	18	9	31
NH_4^+	(0.5809)	(0.1501)	(−0.1856)	0.36	2.7	62	19	2	19
PO_4^{3-}	−0.5944	−0.2824	0.0785	−0.36	–	90	39	6	43
DOC	2.4665	0.1160	−0.1363	0.26	2.7	98	68	6	70
POC	2.7553	1.0028	−0.3166	1.33	–	976	90	9	91
TSS	2.8834	1.0332	−0.3356	1.38	–	976	89	5	90
Guabá									
Alkalinity	2.0420	−0.5566	−0.1195	−0.48	–	91	92	2	92
$Si(OH)_4$	2.2241	−0.4413	−0.0001	−0.44	–	604	93	9	94
Ca^{2+}	1.6255	−0.3463	–	−0.35	–	160	88	9	91
Mg^{2+}	1.4453	−0.2793	–	−0.28	–	158	84	9	90
Na^+	2.3048	−0.1709	−0.0593	−0.13	–	158	83	9	89
Cl^-	2.2502	−0.1525	−0.0619	−0.11	–	640	62	9	72
SO_4^{2-}	1.0949	0.0631	–	0.06	–	155	35	7	59
K^+	1.2366	0.0336	−0.1614	0.14	1.3	324	39	9	34
NO_3^-	0.9760	−0.0644	–	−0.06	–	156	9	7	18
NH_4^+	−0.3132	0.1191	0.0811	0.07	–	60	19	1	25
PO_4^{3-}	(−1.2345)	(0.0191)	(−0.0901)	0.06	2.1	112	4	2	4
DOC	2.3945	0.3563	−0.2427	0.51	5.4	120	65	9	73
POC	2.2507	1.2252	−0.2225	1.37	–	802	86	9	88
TSS	1.9576	1.3838	−0.2103	1.52	–	802	87	8	89
Icacos									
Alkalinity	2.2207	−0.5762	−0.2192	−0.47	–	163	83	6	84

Table 4 continued

Constituent	Regression on all measurements			Regression slope at 50th percentile runoff rate	Runoff rate at peak of arch (mm/h)	Data count	Regression percent variance explained	Best LOADEST model	LOADEST percent variance explained
	a	b	c						
$Si(OH)_4$	2.2176	−0.4805	–	−0.48	–	1062	82	6	82
Ca^{2+}	1.7796	−0.3803	−0.0860	−0.34	–	238	87	9	88
Mg^{2+}	1.5589	−0.3148	−0.0821	−0.27	–	237	86	9	88
Na^{+}	2.2873	−0.1774	−0.0220	−0.17	–	237	72	6	79
Cl^{-}	2.1850	−0.1432	−0.0388	−0.12	–	1,092	39	9	54
SO_4^{2-}	(−1.1857)	(−0.0534)	(0.0571)	0.09	2.9	238	12	6	33
K^{+}	(−1.1983)	(0.0587)	(0.0495)	−0.04	–	607	19	9	24
NO_3^{-}	0.9631	−0.1276	–	−0.13	–	235	26	9	31
NH_4^{+}	(−0.0137)	(−0.0283)	(−0.0015)	0.00	–	136	0	2	3
PO_4^{3-}	[−1.4301]	[0.0090]	–	0.00	–	196	0	1	0
DOC	2.4964	0.4379	−0.3210	0.60	4.8	279	80	9	81
POC	2.1637	1.2957	−0.2307	1.41	–	1,398	89	5	90
TSS	1.8671	1.4909	−0.1749	1.58	–	1,398	90	9	91
Mameyes									
Alkalinity	2.4079	−0.4715	−0.0240	−0.45	–	197	89	6	89
$Si(OH)_4$	2.2669	−0.3455	–	−0.35	–	1,165	59	9	62
Ca^{2+}	2.0662	−0.3699	–	−0.37	–	177	89	4	89
Mg^{2+}	1.7002	−0.2974	–	−0.30	–	177	85	4	86
Na^{+}	2.3216	−0.1969	–	−0.20	–	177	86	8	88
Cl^{-}	2.2533	−0.1404	–	−0.14	–	1,134	33	9	39
SO_4^{2-}	1.4198	−0.1767	–	−0.18	–	179	86	7	87
K^{+}	[1.2590]	[−0.0029]	–	0.00	–	581	0	8	5
NO_3^{-}	1.0023	0.2476	–	0.25	–	178	44	9	54
NH_4^{+}	(−0.1082)	(0.1781)	–	0.00	–	57	10	2	18

Table 4 continued

Constituent	Regression on all measurements			Regression slope at 50th percentile runoff rate	Runoff rate at peak of arch (mm/h)	Data count	Regression percent variance explained	Best LOADEST model	LOADEST percent variance explained
	a	b	c						
PO_4^{3-}	−1.1144	0.3487	0.1188	−0.43	–	141	45	2	45
DOC	2.4841	0.3196	−0.1815	0.45	7.6	164	82	9	85
POC	1.9351	1.1074	−0.1863	1.24	–	1,248	78	8	78
TSS	1.6059	1.2584	−0.2007	1.40	–	1,248	79	8	80

For explanation of best LOADEST model, see Runkel et al. (2004), their Table 7. a indicates constant in regression relating log(concentration) to log(runoff rate), b, linear coefficient in regression relating log(concentration) to log(runoff rate), and c, quadratic coefficient in regression relating log(concentration) to log(runoff rate); *mm/h* millimeters per hour, [] values not statistically different than zero, () regression used LOADEST averages, *DOC* dissolved organic carbon, *POC* particulate organic carbon, *TSS* total suspended solids, – not applicable

Fig. 3 Graph of the slope of the regression of log(runoff rate) to log(concentration) for non-bioactive ▶ constituents compared to the fraction of the constituent yield that is derived from atmospheric deposition. Alkalinity has a negative fractional atmospheric contribution, because atmospheric deposition is naturally acidic, in essence a slight excess of sulfuric and nitric acid (Stallard 2012a). The slope of the regression is evaluated at the 50th percentile of runoff for corresponding river

4.2 Relations Between log(R) and log(C) for Bioactive Constituents

The strongly bioactive constituents typically demonstrate two types of concentration–runoff relations—a nearly constant log(R)–log(C) relation and a concave-down log(R)–log(C) relation (Table 4, Online Resource 1). Sulfate shows a bioactive trend in the Icacos and Guabá rivers, but behaves like a non-bioactive constituent derived from bedrock weathering and atmospheric deposition in the Mameyes, Canóvanas, and Cayaguás rivers. DOC is the archetype for the concave-down relation, with a maximum log(C) at runoff rates between 2.6 and 7.6 mm/h, which Stallard and Murphy (2012) interpret in terms of the composite soil hydrology model. During base flow, most water is presumably arriving through deeper flow paths with less-available bioactive constituents. With increasing runoff, flow paths are shallower; the soil environment is richer in biologically active constituents; and concentrations rise. Rapid flow through macropores and pipes becomes significant. At the highest runoff rates, overland flow becomes important, reducing contact with the soil matrix. Shanley et al. (2011) propose source depletion as an alternative cause for the concave-down log(R)–log(C) relation in the Icacos.

While all bioactive solutes are strongly recycled by plants and retained in shallow soil and biota, only DOC is exclusively derived from gas fixation and released into soil waters from the breakdown of organic matter or as biological exudates. The remaining bioactive constituents are similarly released, but have additional inputs from some combination of bedrock weathering, atmospheric deposition, or fertilizers and/or wastes (some DOC may come from human wastes in the developed watersheds). Moreover, DOC is also the only bioactive constituent with arched log(R)–log(C) relations for all rivers, a characteristic that presumably reflects this narrower suite of sources. The PPA model assumes that weathering products are introduced at a constant rate in proportion to the area of wetted surfaces, and we examine whether that assumption can also be applied to DOC and, by inference, to the introduction of other constituents released from the breakdown of organic matter or as biological exudates.

Assume that the biological reactions that supply bioactive solutes to soil water—decay and biological exudation—are not reversible, are far from equilibrium, and contribute in proportion to wetted surface area. During the initial rising stage, the wetted surface area of DOC sources increases because the concentration of organic matter in soil increases toward the soil surface, and with more sources, DOC concentrations increase. Eventually, as runoff rates rise, an increasing portion of water starts moving through flow paths (macropores, pipes, and eventually overland flow) that limit contact with additional wetted surface. The instantaneous yields of DOC, Y_{DOC} ($Y_{DOC} = R{\cdot}\mathrm{DOC}$), continue to increase, but at a decreasing rate because added water does not wet proportionally as much additional reactive surface. Once the slope of the rate of increase in log(Y_{DOC}) decreases to 1 (note DOC $= Y_{DOC}/R$), DOC starts to decrease; this represents the peak of the log(R)–log(DOC) relation at runoff rates between 2.6 and 7.6 mm/h. Finally, with extreme runoff rates, all possible surfaces become wetted, and any additional water moves through rapid flow paths. Because all possible reactive surfaces are wetted, the instantaneous yield of

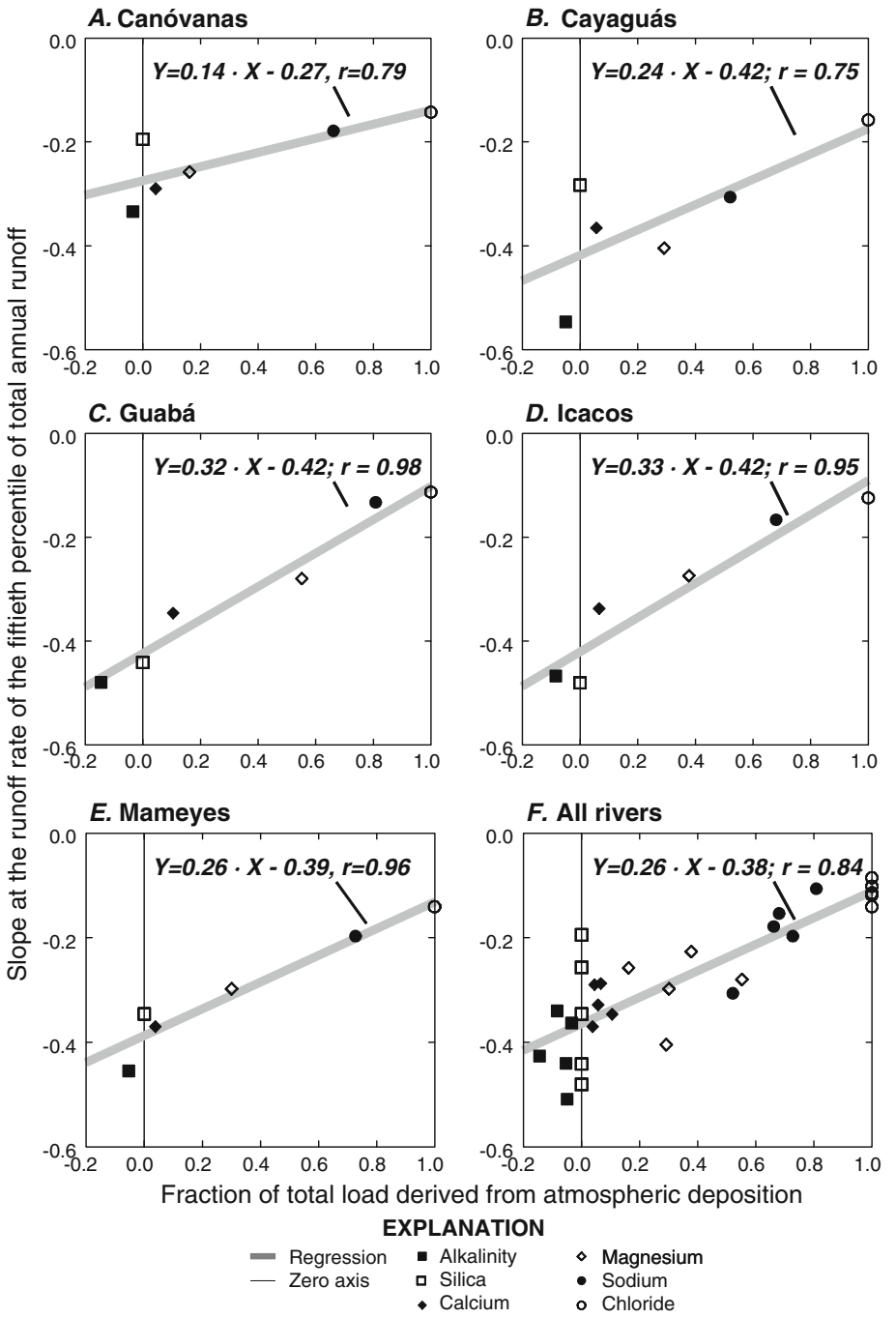

DOC would be at its maximum. An increase in R would not increase Y_{DOC}. This corresponds to a slope of -1 for the log(R)–log(DOC) relation. Accordingly, at highest R, the slope of the log(R)–log(DOC) relation should approach -1 as an asymptote.

Table 5 Average falling stage concentration as a percent change from the rising stage concentration for samples for which the difference between the two averages is significant at greater than a 50 % level

Runoff percentile range	Sample count	Average runoff rate (mm/h)	Alkalinity	$Si(OH)_4$	Ca^{2+}	Mg^{2+}	Na^{+}	Cl^{-}	SO_4^{2-}	K^{+}	NO_3^{-}	DOC	POC	TSS
Canóvanas														
0 to <25	42	0.014	–	–	–	–	–	*−6*	–	–	*30*	–	19	23
25 to <75	182	0.475	**−62**	**−30**	**−60**	**−56**	**−40**	**−22**	*−17*	−5	23	**30**	**−35**	**−37**
75 to <90	230	3.89	**−53**	**−26**	**−40**	**−37**	**−20**	**−17**	**−14**	**−12**	*33*	*7*	**−25**	**−27**
90 to 100	28	9.8	−15	**−15**	−11	−9	−9	*−10*	–	*−15*	−14	−16	–	–
Cayaguás														
0 to <25	110	0.046	–	–	−5	–	–	–	–	*8*	–	–	10	–
25 to <75	92	0.385	**−28**	**−11**	**−27**	**−25**	**−21**	**−9**	*−13*	−4	*64*	−10	−13	−13
75 to <90	131	5.26	**−54**	**−23**	**−51**	**−51**	**−38**	**−16**	−21	**−16**	−36	*−12*	–	–
90 to 100	62	15.6	*−53*	*−12*	−28	−29	**−19**	−9	–	–	–	*−27*	–	11
Guabá														
0 to <25	25	0.062	−10	4	–	–	–	–	–	*−12*	–	16	*−31*	*−34*
25 to <75	33	0.398	6	–	–	–	–	−4	–	–	–	–	*−32*	*−39*
75 to <90	90	2.35	34	**−10**	35	*42*	*28*	–	*28*	−16	–	6	**−52**	**−61**
90 to 100	214	25.0	**−65**	**−11**	**−20**	*−15*	−8	–	–	**−15**	–	**−26**	**−31**	**−33**
Icacos														
0 to <25	31	0.078	–	–	–	–	4	1	6	–	–	16	−9	−26
25 to <75	21	0.421	−9	–	−10	−7	−8	−5	–	−11	–	–	–	–
75 to <90	180	7.19	*−52*	**−33**	**−32**	**−32**	*−15*	**−12**	–	**−9**	–	–	**−23**	**−22**
90 to 100	364	9.37	–	**−23**	*−16*	**−16**	−7	**−11**	–	**−12**	15	**−8**	**−26**	**−26**
Mameyes														
0 to <25	10	0.030	−7	−5	−3	−5	–	–	−2	–	–	*88*	–	–
25 to <75	15	0.488	−28	*−15*	−21	−7	−4	5	*−28*	–	75	53	–	−32
75 to <90	152	4.67	**−33**	**−29**	**−26**	**−25**	*−10*	**−12**	−5	**−13**	−24	8	–	*−15*
90 to 100	283	12.8	*−18*	**−21**	**−22**	**−28**	**−11**	**−12**	**−13**	**−11**	−18	*−16*	–	−5

DOC indicates dissolved organic carbon, *POC* particulate organic carbon, *TSS* total suspended solids, *mm/h* millimeters per hour, italic font, significant (90 %), bold font, highly significant (95 %), – not applicable

The asymptote condition is easily tested for the log(*R*)–log(DOC) relation by using the maximum runoff rates (Table 3) and the regressions for log(DOC) (Table 4). The slope of the log(*R*)–log(DOC) relation at the maximum runoff rate for the Icacos is −0.80 (Fig. 2e) (The Canóvanas has a slope of −0.34; Cayaguás, −0.36; Mameyes, −0.38 and Guabá, −0.61). Thus, all rivers are on log(*R*)–log(DOC) curves approaching the −1 slope asymptote, consistent with this model. During the falling stage, as wetted surface area decreases, the log(*R*)–log(DOC) relation essentially retraces the rising stage relation. The DOC yield at maximum *R* for the Icacos is 12 k mol carbon (144 kilograms carbon)/km^{2}h.

Nothing in these data suggests a more pronounced chemostatic behavior of the nutrients typically applied as fertilizers (K^+, NO_3^-) in the agricultural watersheds compared with forested watersheds (Table 4, Online Resource 1), as proposed by Basu et al. (2010) and Thompson et al. (2011). The elevated yields (Stallard and Murphy 2012) indicate either legacy inputs or continued use in agricultural watersheds, but if anything, the nutrients in these watersheds demonstrate more arched and less chemostatic relations. In light of the DOC model just proposed, significant reservoirs of these nutrients in the shallowest soils are indicated.

The strongly bioactive constituents typically demonstrate two types of hysteresis. Constituents with significant bedrock weathering contributions, specifically K^+ in all watersheds and SO_4^{2-} in the Mameyes, Canóvanas, and Cayaguás watersheds, show a clockwise hysteresis with similar magnitude to those of the non-bioactive constituents (Table 5). We interpret this hysteresis similarly to that of non-bioactive constituents, reflecting the influence of riparian areas and perhaps hyporheic flow. For NO_3^- (and SO_4^{2-} in the Icacos and Guabá rivers), there is generally little statistically significant hysteresis, or even higher concentrations on the falling stage than the rising stage. For DOC, all rivers showed slight but significant clockwise hysteresis at the highest runoff rates (90–100th percentile); the Cayaguás also has moderately significant clockwise hysteresis for DOC in the 25–75th and 75–90th percentiles.

If a flood plain component is assumed to be important for the other constituents, why would it be largely absent for NO_3^- and DOC? A considerable portion of NO_3^- and all of DOC are ultimately derived through biological fixation from atmospheric gases and retained as various forms of organic carbon and nitrogen in the uppermost parts of the soil profile or on the soil surface. Anoxic parts of riparian zones can transform NO_3^- through denitrification and ammonification, thereby decreasing its concentration (McDowell et al. 1992, 1996), so clockwise hysteresis caused by a flood plain component would be unlikely. DOC processing by flood plains in eastern Puerto Rico is not as well studied, but plants and soil organic matter, the source of DOC in shallow flow paths, are similarly abundant in shallow-soil areas, including on flood plains (McDowell et al. 1992; Zarin and Johnson 1995). Therefore, there is no obvious reason to expect large differences in DOC concentrations in a riparian component. The exception provided by DOC in the Cayaguás may support this general argument. The Cayaguás has the most extensive flood plain and most deforested uplands of all the rivers (Murphy et al. 2012). There may indeed be a sufficient contrast in sources of organic matter in these two settings to drive hysteresis in the Cayaguás watershed.

4.3 Relations Between log(*R*) and log(*C*) for Particulate Constituents

The two particulate components that were studied, POC and suspended solids, have broadly similar log(*R*)–log(*C*) relations in all rivers; in each river, hysteresis is similar for both constituents, but differs considerably from other rivers (Table 5). In all cases of a

significant difference between rising stage and falling stage concentrations (Canóvanas, Icacos, and Guabá rivers), the rising stage concentrations are greater, an indication of a dominance of clockwise loops described in sediment studies (Williams 1989). Unlike the other rivers, the Guabá shows a significant hysteresis at all runoff rates, indicating that remobilization of material deposited on the rock bed is always occurring, even at low-flow conditions (as is obvious during field visits). Gellis (2012) recently applied a derivative of the Williams (1989) schema to four rivers in eastern Puerto Rico (only the Icacos watershed is shared between Gellis 2012 and the WEBB study). Gellis (2012) shows that for the Icacos, Q/C loops are dominantly clockwise. He found a mix of clockwise and counterclockwise loops in two agricultural watersheds and dominantly counterclockwise loops in an urban watershed. These results are consistent with those of the current study.

5 Conclusions

1. An examination of the relation between log(R) and log(C) for non-bioactive solutes allows the distinction of a dominantly bedrock weathering source (slope −0.3 to −0.4) and a source derived from atmospheric deposition and subsequent evapotranspiration (slope −0.1). The respective slopes of these relations are similar for all watersheds and constituents. Differences in the slope of the relation among constituents depend on the relative importance of bedrock weathering and atmospheric deposition as sources. This constancy of slope, b, for the bedrock-derived components is essentially a validation of the Godsey et al. (2009) "permeability-porosity-aperture" (PPA) model for this landscape. This may be the most rigorous test of the PPA model possible, and those authors caution that "any such attempt at direct measurement (of the properties that go into determining the slope) would be complicated by the spatial heterogeneity in subsurface properties, as well as the large differences between field and laboratory weathering rates." We cannot use the chemostat metric of Thompson et al. (2011) because our runoff range is too broad and not normally distributed. And, the approach of Basu et al. (2010), when compared to the similar calculations done by Stallard (2012b), would classify every constituent as being chemostatic.
2. The arched log(R)–log(C) relations for many of the bioactive constituents, particularly DOC, and the lack of open clockwise hysteresis indicate that source depletion does not drive this arched relation. The peak of the arch (which, for DOC, occurs at runoff rates between 2.6 and 7.6 mm/h) is interpreted as representing a transition from dominantly soil-matrix flow to near-surface macropore flow, and finally to overland flow. At the highest R, wetting of all possible reactive surfaces has occurred, resulting in a constant rate of input of C independent of R. The slope approaches an asymptote of −1 at the highest runoff values. For non-bioactive constituents, highest runoff rates should not strongly affect the log(R)–log(C) relations, because near-surface soils are depleted in these constituents. For DOC, the observed arching reduces the DOC yield compared to that estimated through extrapolation using low-runoff-rate data (Stallard 2012b); if this conceptual model applies generally, then tropical montane DOC fluxes are generally overestimated.
3. Both the simple linear log(R)–log(C) relations for non-bioactive constituents and the arched relations for bioactive constituents are consistent with a three-stage composite model of runoff generation. At lower runoff rates, water is flowing through deeper soil. Concentrations drop for the non-bioactive constituents, reflecting a lack of near-surface sources other than the atmospheric deposition itself. The concentrations of

bioactive constituents typically rise, reflecting their greater presence in near-surface soil horizons.

4. The systematic and unified pattern of response demonstrated by these five rivers leads us to propose that other montane watersheds in the humid tropics should demonstrate similar three-stage responses. These observations support extending the PPA model of Godsey et al. (2009), which describes log(R)–log(C) relations based on simplified soil physics and weathering chemistry, to include parameterization of (1) atmospheric inputs that are concentrated in soil waters by evapotranspiration, (2) macropore flow and overland flow in a way that recognizes the role of supply limitation of shallow-soil inputs with increasing runoff rates, and (3) biological processes (decay and biological exudation) that includes recognition of the unidirectional nature and rate limitations typical of such processes. The PPA model assumption that solute supply is directly related to wetted surface area of reactants is the important feature of the model, and it appears to work at high runoff rates where other model assumptions break down. No other tropical watersheds have been studied at sufficiently high runoff rates to permit this comparison at this time.
5. The presence of clockwise hysteresis, but no open loops, over a wide range of runoff rates for the non-bioactive constituents and the bioactive constituents with bedrock weathering and atmospheric sources in the four rivers with flood plains, riparian zones, or thick bouldery beds with a good potential for hyporheic flow, and the lack of this hysteresis in the river without any of these features, suggests that displacement of water from such zones during either rising or falling stages may cause this hysteresis.
6. Suspended sediment and POC demonstrate only clockwise hysteresis in some rivers at high runoff rates. Only the Guabá has a significant hysteresis at all flows, indicating that at low flow, mobilization of material from its rock bed may be important.

Acknowledgments We thank all of our colleagues who have helped with this research, far too many to list here. This work was supported by the US Geological Survey, primarily the Water Mission Area's National Research Program and the Climate and Land Use Change Mission Area. Doug Burns and two anonymous reviewers provided many helpful suggestions and comments.

References

Alexander RB, Slack JR, Ludtke AS, Fitzgerald KK, Shertz TL (1996) Data from selected U.S. Geological Survey national stream water quality monitoring networks. US Geol Surv Digital Data Ser DDS–37 2 CD-ROM

Baedecker MJ, Friedman LC (2000) Water, energy, and biogeochemical budgets—a watershed research program. US Geol Surv Fact Sheet 165–99

Basu NB, Destouni G, Jawitz JW, Thompson SE, Loukinova NV, Darracq A, Zanardo S, Yaeger M, Sivapalan M, Rinaldo A, Rao PSC (2010) Nutrient loads exported from managed catchments reveal emergent biogeochemical stationarity. Geophys Res Lett 37:L23404. doi:10.1029/2010GL045168

Beven KJ, Germann P (1982) Macropores and water flows in soils. Water Resour Res 18:1311–1325

Bevington PR, Robinson KD (2003) Data reduction and error analysis for the physical sciences, 2nd edn. McGraw Hill, New York

Bricker OP, Godfrey AE, Cleaves ET (1968) Mineral-water interactions during the chemical weathering of silicates, in trace inorganics in water. In: Gould RF (ed) Advances in chemistry series 73. American Chemical Society, Washington, pp 128–142

Brooks JR, Barnard HR, Coulombe R, McDonnell J (2010) Ecohydrologic separation of water between trees and streams in a Mediterranean climate. Nat Geosci 3:100–104. doi:10.1038/NGEO722

Burns DA, McDonnell JJ, Hooper RP, Peters NE, Freer JE, Kendall C, Beven K (2001) Quantifying contributions to storm runoff through end-member mixing analysis and hydrologic measurements at the Panola mountain research watershed (Georgia, USA). Hydrol Process 15:1903–1924

Chanat JG, Rice KC, Hornberger GM (2002) Consistency of patterns in concentration-discharge plots. Water Resour Res 38.doi: 10.1029/2001WR000971

Chappell NA, Sherlock MD (2005) Contrasting flow pathways within tropical forest slopes of ultisol soils. Earth Surf Process Landf 30:735–753

Chappell NA, Franks SW, Larenus J (1998) Multi-scale permeability estimation for a tropical catchment. Hydrol Process 12:1507–1523

Christophersen N, Neal C, Hooper RP, Vogt RD, Andersen S (1990) Modelling stream water chemistry as a mixture of soil water end-members—a step towards second-generation acidification models. J Hydrol 116:307–320

Cleaves ET, Godfrey AE, Bricker OP (1970) Geochemistry of a small watershed and its geomorphic implications. Geol Soc Am Bull 85:3015–3032

Elsenbeer H (2001) Hydrologic flow paths in tropical rainforest soils capes—a review. Hydrol Process 15:1751–1759

Evans C, Davies TD (1998) Causes of concentration/discharge hysteresis and its potential as a tool for the analysis of episode hydrochemistry. Water Resour Res 34:129–137

Gellis AC (2012) Factors influencing storm-generated suspended-sediment concentrations and loads in four basins of contrasting land use, humid-tropical Puerto Rico. Catena. doi:10.1016/j.catena.2012.10.018

Godsey SE, Elsenbeer H, Stallard RF (2004) Overland flow generation in two lithologically distinct rainforest watersheds. J Hydrol 295:276–290

Godsey SE, Kirchner JW, Clow DW (2009) Concentration-discharge relationships reflect chemostatic characteristics of US watersheds. Hydrol Process 23:1844–1864

Goldsmith ST, Carey AE, Lyons WB, Kao S-J, Lee T-Y, Chen J (2008) Extreme storm events, landscape denudation, and carbon sequestration: typhoon Mindulle, Choshui River. Taiwan Geol 36:483–486

Haire WJ (1972) Flood of October 5–10, 1970 in Puerto Rico. Commonw Puerto Rico Water Resour Bull 12

Hicks DM, Gomez B, Trustrum MA (2000) Erosion thresholds and suspended sediment yields, Waipaoa River Basin, New Zealand. Water Resour Res 36:1129–1142

Hooper RP, Christophersen N, Peters NE (1990) Modelling stream water chemistry as a mixture of soil water end-members—an application to the Panola mountain catchment, Georgia, USA. J Hydrol 116:321–343

Jones JAA (1990) Piping effects in humid lands. In: Higgins CG, Coates DR (eds) Groundwater geomorphology. Geol Soc Am Special Paper 252: 111–138

Kurtz AC, Lugolobi F, Salvucci G (2011) Germanium-silicon as a flow path tracer: application to the Rio Icacos watershed. Water Resour Res 47:W06516

Larsen MC (1997) Tropical geomorphology and geomorphic work-A study of geomorphic processes and sediment and water budgets in montane humid-tropical forested and developed watersheds. Dissertation University of Colorado, Puerto Rico

Larsen MC (2012) Landslides and sediment budgets in four watersheds in eastern Puerto Rico. In: Murphy SF, Stallard RF (eds) Water quality and landscape processes of four watersheds in eastern Puerto Rico. US Geol Surv Prof Pap 1789-F:153–178

Larsen MC, Torres-Sánchez AJ, Concepción IM (1999) Slopewash, surface runoff, and fine litter transport in forest and landslide scars in humid tropical steep lands, Luquillo experimental forest, Puerto Rico. Earth Surf Process Landf 24:481–506

Larsen MC, Liu Z, Zou X (2012) Effects of earthworms on slope wash, surface runoff, and fine-litter transport on a humid tropical forested hillslope, Luquillo experimental forest, Puerto Rico. In: Murphy SF, Stallard RF (eds) Water quality and landscape processes of four watersheds in eastern Puerto Rico: US Geol Surv Prof Pap 1789- G:179–197

McDowell WH, Bowden WB, Asbury CE (1992) Riparian nitrogen dynamics in two geomorphologically distinct tropical rain forest watersheds—subsurface solute patterns. Biogeoch 18:53–75

McDowell WH, McSwiney CP, Bowden WB (1996) Effects of hurricane disturbance on groundwater chemistry and riparian function in a tropical rain forest. Biotropica 28:577–584

Murdoch PS, McHale MR, Mast MA, Clow DW (2005) The US geological survey hydrologic benchmark network.US Geol Surv Fact Sheet 2005–3135

Murphy SF, Stallard RF (eds) (2012a) Water quality and landscape processes of four watersheds in eastern Puerto Rico. US Geol Surv Prof Pap 1789. http://pubs.usgs.gov/pp/1789/. Accessed 26 November 2012

Murphy SF, Stallard RF (2012b) Hydrology and climate of four watersheds in eastern Puerto Rico. In: Murphy SF, Stallard RF (eds) Water quality and landscape processes of four watersheds in eastern Puerto Rico. US Geol Surv Prof Pap 1789-C:43–84

Murphy SF, Stallard RF (2012c) Methods used to analyze water quality of four watersheds in eastern Puerto Rico—Appendix 2. In: Murphy SF, Stallard RF (eds) Water quality and landscape processes of four watersheds in eastern Puerto Rico. US Geol Surv, USGS Prof Pap 1789:289–292

Murphy SF, Stallard RF, Larsen MC, Gould WA (2012) Physiography, geology, and land cover of four watersheds in eastern Puerto Rico. In: Murphy SF, Stallard RF (eds) Water quality and landscape processes of four watersheds in eastern Puerto Rico. US Geol Surv Prof Pap 1789-A:1–24

Runkel RL, Crawford CG, Cohn TA (2004) Load estimator (LOADEST): a FORTRAN program for estimating constituent loads in streams and rivers. US Geol Surv Tech Methods Book 4

Schellekens J, Scatena FN, Bruijnzeel LA, van Dijk AIJM, Groen MMA, van Hogezand RJP (2004) Storm flow generation in a small rainforest catchment in the Luquillo experimental forest, Puerto Rico. Hydrol Process 18:505–530

Shanley JB, McDowell WH, Stallard RF (2011) Long-term patterns and short-term dynamics of stream solutes and suspended sediment in a rapidly weathering tropical watershed. Water Resour Res 47 doi:10.1029/2010WR009788

Simon A, Larsen MC, Hupp CR (1990) The role of soil processes in determining mechanisms of slope failure and hillslope development in a humid-tropical forest, eastern Puerto Rico. In: Kneuper PLK, McFadden LD (eds) Soils and landscape evolution. Geomorphol 3:263–286

Stallard RF (1985) River chemistry, geology, geomorphology, and soils in the Amazon and Orinoco basins. In: Drever JI (ed) The chemistry of weathering. NATO ASI Series C—Math Phys Sci 149. Reidel, Dordrecht pp 293–316

Stallard RF (2012a) Atmospheric inputs to watersheds in the Luquillo Mountains of eastern Puerto Rico. In: Murphy SF, Stallard RF (eds) Water quality and landscape processes of four watersheds in eastern Puerto Rico. US Geol Surv Prof Pap 1789-D:85–112

Stallard RF (2012b) Weathering, landscape equilibrium, and carbon in four watersheds in eastern Puerto Rico. In: Murphy SF, Stallard RF (eds) Water quality and landscape processes of four watersheds in eastern Puerto Rico. US Geol Surv Prof Pap 1789-H:199–248

Stallard RF (2012c) Data processing and computation to characterize hydrology and compare water quality of four watersheds in Puerto Rico—Appendix 1. In: Murphy SF, Stallard RF (eds) Water quality and landscape processes of four watersheds in eastern Puerto Rico. US Geol Surv, USGS Prof Pap 1789:263–287

Stallard RF, Murphy SF (2012) Water quality and mass transport in four watersheds in eastern Puerto Rico. In: Murphy SF, Stallard RF (eds) Water quality and landscape processes of four watersheds in eastern Puerto Rico. US Geol Surv Prof Pap USGS Prof Pap 1789-E:113–152

Thompson SE, Basu NB, Lascurain Jr J, Aubeneau A, Rao PSC (2011), Relative dominance of hydrologic versus biogeochemical factors on solute export across impact gradients. Water Resour Res 47 W00J05 doi:10.1029/2010WR009605

Williams GP (1989) Sediment concentration versus water discharge during single hydrologic events. J Hydrol 111:89–106

Wolman MG, Gerson R (1978) Relative scales of time and effectiveness of climate in watershed geomorphology. Earth Surf Process 3:189–208

Wolman MG, Miller JP (1960) Magnitude and frequency of forces in geomorphic processes. J Geol 68:54–74

Zarin DJ, Johnson AH (1995) Base saturation, nutrient cation, and organic matter increases during early pedogenesis on landslide scars in the Luquillo experimental forest, Puerto Rico. Geoderma 65(3–4):317–330